


Article

# Cognitive Risk-Assessment and Decision-Making Framework for Increasing in-Vehicle Intelligence

George Dimitrakopoulos \*, Elena Politi , Konstantina Karathanasopoulou, Elias Panagiotopoulos and Theodore Zographos

Department of Informatics & Telematics, Harokopio University of Athens, 9, Omirou Str., Tavros, 17778 Athens, Greece

\* Correspondence: gdimitra@hua.gr

**Abstract:** The key challenge for future automated driving systems is the need to imitate the intelligence and ability of human drivers, both in terms of driving agility, as well as in their intuitive understanding of the surroundings and dynamics of the vehicle. In this paper a model that utilizes data from different sources coming from vehicular sensor networks is presented. The data is processed in an intelligent manner while integrating knowledge and experience associated with potential and any decision. Moreover, the appropriate directives for the safety of the vehicle as well as alerts in case of upcoming emergencies are provided to the driver. The innovation lies in attributing human-like cognitive capabilities—non-causal reasoning, predictive decision-making, and learning—integrated into the processes for perception and decision-making in safety-critical autonomous use cases. The overall approach is described and formulated, while a heuristic function is proposed for assisting the driver in reaching the appropriate decisions. Comprehensive results from our experiments showcase its efficiency, simplicity, and scalability.

**Keywords:** in-vehicle intelligence; safety; emergency management; risk management proactive; cognitive



**Citation:** Dimitrakopoulos, G.; Politi, E.; Karathanasopoulou, K.; Panagiotopoulos, E.; Zographos, T. Cognitive Risk-Assessment and Decision-Making Framework for Increasing in-Vehicle Intelligence. *J. Sens. Actuator Netw.* **2022**, *11*, 72. <https://doi.org/10.3390/jsan11040072>

Academic Editor: Javier Alonso Ruiz

Received: 9 August 2022

Accepted: 13 October 2022

Published: 31 October 2022

**Publisher's Note:** MDPI stays neutral with regard to jurisdictional claims in published maps and institutional affiliations.



**Copyright:** © 2022 by the authors. Licensee MDPI, Basel, Switzerland. This article is an open access article distributed under the terms and conditions of the Creative Commons Attribution (CC BY) license (<https://creativecommons.org/licenses/by/4.0/>).

## 1. Introduction

The rapid growth of the population in urban areas as well as the increased number of vehicles create numerous disruptions for transportation systems as well as the environment, such as traffic congestion, air pollution, noise, and many more. Moreover, problems such as traffic diversion and the diversity of the urban environment may compromise safety in driving. Such problems seriously affect the economy when considered as a whole [1]. To address the above challenges, the ecosystem of a smart city introduces intelligent solutions, such as the continuous monitoring and management of infrastructure, the rise of intelligent transportation systems, and many more. Moreover, the EU has implemented a roadmap, namely the European Green Deal which aims at a target of 55% lower CO<sub>2</sub> emissions by 2030 [2]. This roadmap puts a major effort into “digital technologies” such as AI-based solutions, or energy storage systems that can offer sustainability for the usage of future vehicles, endowing them with several degrees of intelligence.

Among others, mobility and transportation are the areas to be benefited from the European Green Deal. In fact, the accelerated rise of new technologies, changing consumer preferences and emerging mobility services are drastically transforming the automotive industry. This moment of change is driven by the race to deliver sustainable digital mobility. The digital transformation in the automotive industry requires that all players in the digital automotive value chain seek to benefit from innovations enabled by software and electronics. To keep pace with this, appropriate initiatives that will assure that digital technologies will accelerate and transform the state of future vehicles are taken in the EU.

While the concept of digital transformation in the mobility and transportation areas is associated with four major trends, namely electrification, standardization, automatization,

and digitalization, for the automotive sector, these mobility trends are translated into electric, connected, autonomous, and shared (ECAS) vehicles [2–4]. In this context, it is expected that ECAS vehicles will offer new mobility services with scaled-down ecological footprint while offering extended safety, security, reliability, availability, and affordability in driving.

Moreover, recent advances in the area of Connected, Cooperative, and Automated Mobility (CCAM) have facilitated communication among vehicles (V2V), as well as between vehicles and roadside units (also referred to, as “infrastructure”) (V2I). Additionally, a valid facilitator of V2V and V2I communications is the imitation of the intelligence and ability of human drivers, both in terms of driving agility, as well as in their intuitive understanding of the surroundings and dynamics of the vehicle. This paper aims to tackle exactly this challenge by proposing a framework that enables vehicles to exercise human-like cognitive capabilities across the sense-plan-act chain, for perception and decision-making. In this respect, its main contribution is that it builds upon previous research attempts (e.g., Ref. [5]), adding functionality that comprises global protection, an early warning algorithm for vehicles, based on a priori risk assessment that serves as an input to autonomous decision making, all equipped with knowledge and experience that promotes driver safety drivers at a significant level. The main benefit of the proposed framework, namely “Autonomous Safety Management” (ASM) is its smooth deployment, based on the existing 4G/5G mobile communication network. Moreover, the algorithms are simple, easily deployable (multithreaded, SIMD, etc.), and of low energy requirements. In summary, the ASM framework is effective, available, and scalable.

The rest of the paper is as follows. In Section 2, the motivation for this work based on related research efforts is presented, together with a high-level description of ASM. Section 3 presents the mathematical formulation of the problem and describes the heuristic utilized for its solution. Section 4 presents the comprehensive results of our study obtained through a series of simulations. Finally, conclusions and next steps are summarized in Section 5.

## 2. Motivation and High-Level Description

### 2.1. Intelligent Vehicles

Research in embedded intelligence in vehicles has been long focused on the real-time assessment of traffic [6–8], safety management for the vehicle and the surrounding environment including Vulnerable Road Users (VRUs) [9], the modeling of driver behavior [10], the (a priori) handling of forthcoming emergencies [11,12], the management of the vehicle environmental behavior [13], as well as the utilization of AI tools and methods for enriching sensor technologies behavior [14–16]. Last, the relaying of crucial information to the driver has also been the subject of research [17,18].

### 2.2. Risk Assessment

In particular, there exist several multi-disciplinary and interactive factors that affect the reliability of decisions taken by an intelligent vehicle, such as network architectures, hardware fault tolerance, resilient machine learning, human-machine interactions, perception of dynamic environments, and many more. A number of works have been proposed for assessing the potential risks related to intelligent vehicles [19]. There are a few methods to analyze failure, manage uncertainties, and predict the reliability of Autonomous Vehicles (Avs) [20,21]. Some widely known methods focused on analyzing failure, and predicting reliability are the Time to Failure (TTF), Interval Analysis (IA), Fault Tree Analysis (FTA), Root Cause Analysis (RCA), Failure Mode and Effect Analysis (FMEA), and Failure Mode Effects and Criticality Analysis (FMECA). The Failure Mode and Effects Analysis (FMEA), which we adapt in this paper, is an engineering method that helps to identify weak points during the concept and design phase of all kinds of products (hardware, software) and processes [22]. In engineering practice, FMEA is commonly implemented at the early stage of system development such that critical system components and potential failures and

risks can be identified early. According to the FMEA rationale, each risk can be assessed through the production of its severity (on a scale of 0–10, 10 being the most severe), occurrence probability (on a scale of 0–10, 10 being the most probable), and detectability (in a scale 0–10, 10 being the easiest to detect) [23]. Furthermore, FMEA can be further enhanced to classify the failure modes based on the probability of failure.

### 2.3. High-Level Description

This paper builds on the above research efforts, taking them several steps forward, through:

- (a) assessing traffic information in a real-time manner through aggregating and federating information from sensors embedded in the vehicle,
- (b) considering a set of potential decisions applying a novel, cognitive heuristic
- (c) associating each of the candidate’s decisions with potential risks and therefore influencing the solutions space,
- (d) increasing the embedded intelligence of a vehicle through a holistic safety approach, with the use of in-vehicle sensors

Figure 1 shows the ASM scheme operates. A wireless sensor network utilizes the aggregated data and through an efficient heuristic, it sends an alert to the driver in case of an emergency situation, so that specific actions can be taken. The sensors are located in specific positions on the vehicle, in adjacent vehicles, or in key positions of the infrastructure, such as traffic lights or road signs.

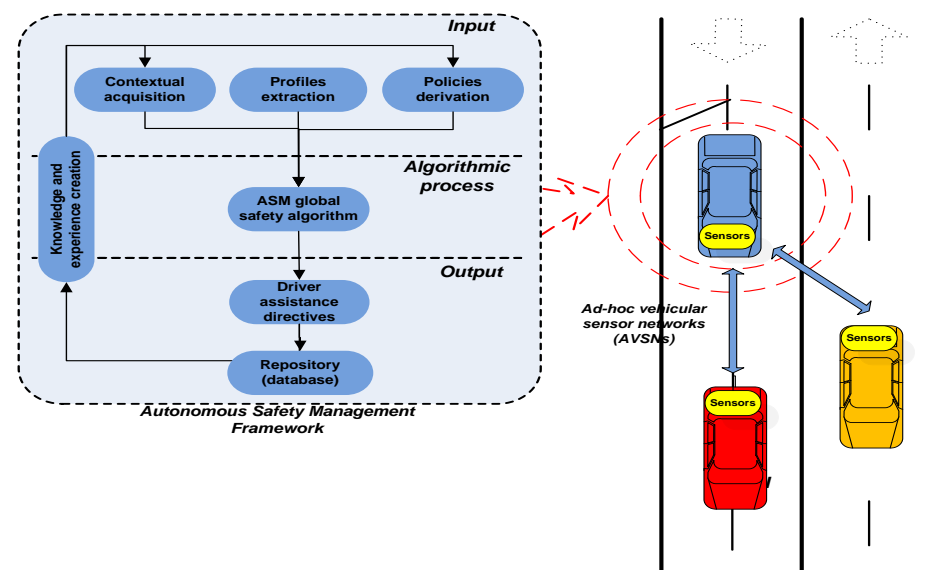


Figure 1. ASM high-level description.

The following section presents the details of the framework.

## 3. Problem Description and Solution

### 3.1. Context Modeling

This section describes the context of the simulation. Our paper utilizes an approach that envisages the existence of a set of vehicles that comprise an ad-hoc vehicular network, whereas there is a center vehicle that constitutes the one that has integrated the proposed framework and tries to federate information from its neighboring vehicles. This vehicle integrates the available road network Geographic Information System (GIS) data (that is publicly available, such as OSM, TIGER 2014) or data aggregated from the ASM framework, as well as computing and processing capabilities for analyzing those data. Figure 2 reflects the functional architecture for this process.

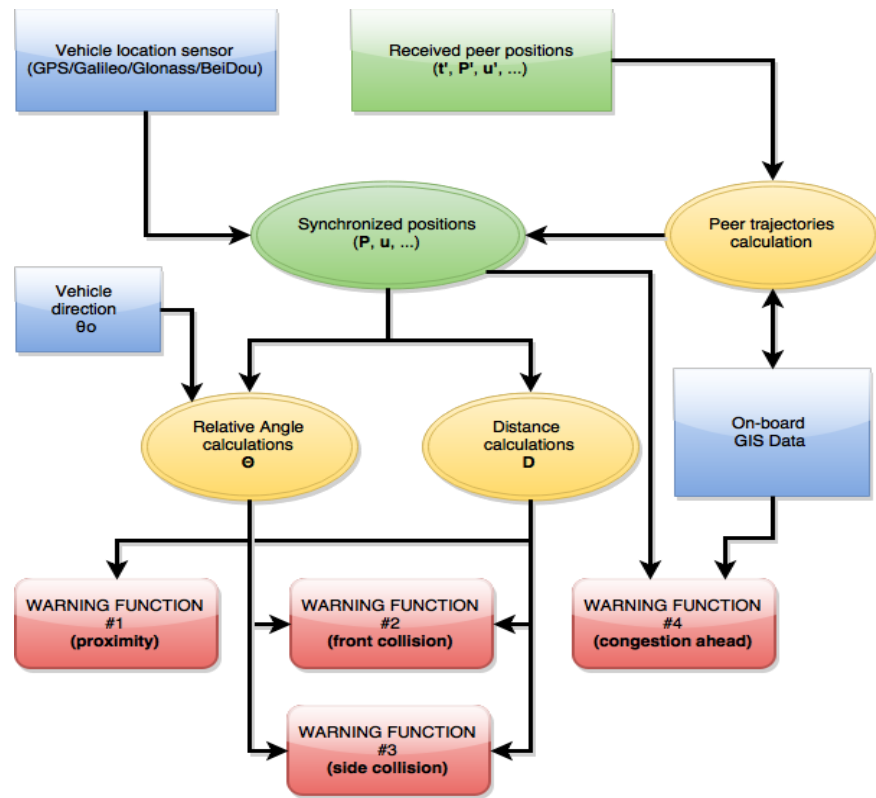


Figure 2. Functional block-diagram.

In our approach, we assume that the vehicle dimensions are negligible, while their position is considered as a point in the navigation space. The set of vehicles is given by:  $V = \{v_1, v_2, \dots, v_N\}$ , where  $N$  is the number of vehicles in the network.

If the vector  $\hat{v}_0$  represents the direction of the vehicle  $v_0$ , starting from the center of mass of the vehicle where  $v_0$  is the reference vehicle and motion is considered a straight line, as illustrated in Figure 3 vector  $\overline{V}_0 = \{\overline{v}_0v_1, \overline{v}_0v_2, \dots, \overline{v}_0v_N\}$  describes the set of sub-vectors, starting from  $v_0$  and ending at each of  $v_i, i \in N$ . The  $v$

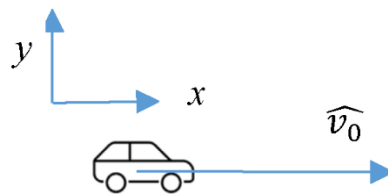


Figure 3. Motion of the vehicle.

Next, we calculate the distances  $D$  between the reference vehicle and every other vehicle in the network given by Equation (1):

$$D = |\overline{V}_0| = \{|\overline{v}_0v_1|, |\overline{v}_0v_2|, \dots, |\overline{v}_0v_N|\} \tag{1}$$

In order to find the set of angles  $\Theta$  between the subject vehicle’s direction and every other vehicle in the network, we consider the following set of dot products, given by Equation (2):

$$\hat{v}_0 \cdot \overline{V}_0 = |\hat{v}_0| |\overline{V}_0| \cos(\widehat{\hat{v}_0 \cdot \overline{V}_0}) = D \cos \Theta \tag{2}$$

where every operator and function is applied to each element of the set respectively. Therefore Equation (3):



$$\Theta = \arccos\left(\frac{\hat{v}_0 \cdot \bar{V}_0}{D}\right) = \left\{ \arccos\left(\frac{\hat{v}_0 \cdot \bar{v}_0 \cdot \bar{v}_i}{|\bar{v}_0 \cdot \bar{v}_i|}\right), \forall i \in N \right\} \left\{ \arccos\left(\frac{\hat{v}_0 \cdot \bar{v}_0 \cdot \bar{v}_i}{|\bar{v}_0 \cdot \bar{v}_i|}\right), \forall i \in N \right\} \quad (3)$$

The set of vectors  $\bar{V}_0$  can be calculated by using the geodetic coordinates of each vehicle via accurate location sensors, such as multi-constellation GPS/GLONASS/Galileo/BeiDou GNSS receivers [23], LTE (4G), etc., on a reference (established) datum (ellipsoid with an offset and a rotation), e.g., WGS84. Every pair of geodetic coordinates corresponds to exactly one pair of Cartesian coordinates, using the UTM plane coordinate grid system [24].

We then consider  $P$  as the set containing the Cartesian coordinates of every peer vehicle, such that Equation (4):

$$P = \{(x_i, y_i), \forall i \in N\} \quad (4)$$

Let  $\theta_0$  be the direction (azimuth) of the subject vehicle on the Cartesian plane. The unit vector  $\hat{v}_0$  can be expressed as Equation (5):

$$\hat{v}_0 = \cos(\theta_0)\hat{x} + \sin(\theta_0)\hat{y} = \begin{bmatrix} \cos \theta_0 \\ \sin \theta_0 \end{bmatrix} \quad (5)$$

The  $i$ -th element of the sets  $D$  and  $\Theta$  can be written as Equation (6):

$$d_i = \sqrt{(x_i - x_0)^2 + (y_i - y_0)^2}, \forall i \in N \text{ and:}$$

$$\theta_i = \arccos\left(\frac{\begin{bmatrix} \cos \theta_0 \\ \sin \theta_0 \end{bmatrix} \cdot \begin{bmatrix} x_i - x_0 \\ y_i - y_0 \end{bmatrix}}{\sqrt{(x_i - x_0)^2 + (y_i - y_0)^2}}\right), \forall i \in N \quad (6)$$

Although mathematically correct, the aforementioned formula can pose several difficulties in calculations, in case of angles near the flat extrema of the inverse cosine function, or because of the square root of distances [25].

A more computationally accurate method for calculating the set of angles  $\Theta$  would be to combine the vectors  $\hat{v}_0$  and  $\bar{V}_0$  as follows Equation (7):

$$\hat{v}_0 \times \bar{V}_0 = |\hat{v}_0| |\bar{V}_0| \sin(\widehat{\hat{v}_0 \cdot \bar{V}_0}) \hat{k} = D \sin \Theta \cdot \hat{k} \quad (7)$$

where  $\hat{k}$  the unit vector perpendicular to the 2D surface defined by vectors  $\hat{v}_0$  and  $\bar{V}_0$ . Dividing with the dot product and substituting with the Cartesian coordinates of vectors, we get:

The set  $\Theta$  can be derived by using the well-known atan2 function, present in most modern programming languages.

### 3.2. Solution Approach: Warning Functions

To enhance decision-making capabilities, our framework may calculate a warning function  $F$  which may take the sets  $D$ ,  $\Theta$ , and  $P$  as input for every point and map them to a set of warning level values  $W$ , as shown below. The set can be a crisp set or a fuzzy set, given by Equation (8).

$$F : (D, \Theta, P, \dots) \mapsto W, W = \{w_j, j = 1, 2, \dots\} \quad (8)$$

The results of the aforementioned function are updated for every point of the vehicle navigation. Next, some of the aforementioned functions will be presented as well as a statistical analysis using a simulated traffic environment.

The last step for reaching decisions is risk assessment. In particular, the proposed framework has the ability to associate each candidate’s decision with a set of risks and therefore decreasing accordingly the solution space (i.e., a highly risky decision will not be implemented). In this paper, we will extend our work presented in Ref. [26], in which the algorithm took as input pieces of information from the driver layer and the environmental layer. After simulations, the algorithm calculated the Risk severity, risk occurrence probability, and risk priority number regarding the potential failure mode.

According to Ref. [26], the result is the identification of a number of critical components in CR-LOA, based on the aforementioned risk priority number (RPN) as shown in Equation (9), i.e.,

$$RPN_i = S_i \times P_i \times D_i \quad (i = 1, 2, \dots, N) \tag{9}$$

where  $N$  refers to the total number of failure modes of the CR-LOA components being considered;  $S_i$ ,  $P_i$ , and  $D_i$  describe the severity level, failure probability, and detectability of the failure of the  $i$ -th potential failure mode, respectively. In principle, the higher the RPN, the more critical the corresponding failure mode of the ‘i-AP’ component becomes. Overall, the severity level  $S_i$  and detectability  $D_i$  are assessed based on the method depicted in Table 1, while the failure probability  $P_i$  and overall risk mitigation probability are assessed based on the ranges listed in Table 2.

**Table 1.** Detectability Assessment Table.

Detection	Likelihood of Detection	Di Ranking	Status
Absolute uncertainty	Design control cannot detect potential cause/ mechanism	10	Red
Very remote	Very remote chance the control will detect potential cause/ mechanism	9	Red
Remote	Remote chance the control will detect potential cause/ mechanism	8	Red
Very low	Very low chance the control will detect potential cause/ mechanism	7	Red
Low	Low chance the control will detect potential cause/ mechanism	6	Red
Moderate	Moderate chance the control will detect potential cause/ mechanism	5	Yellow
Moderately high	Moderately high chance the control will detect potential cause/ mechanism	4	Yellow
High	High chance the control will detect potential cause/ mechanism	3	Green
Very high	Very high chance the control will detect potential cause/ mechanism	2	Green
Almost certain	Almost certain the control will detect potential cause/ mechanism	1	Green

**Table 2.** Risk Priority Number (RPN) Assessment.

Risk Priority Number	Risk Mitigation Possibility
513–1000	Very High
217–512	High
65–216	Medium
9–64	Low
0–8	Improbable

Let it be noted that an FMEA-oriented algorithmic process for in-vehicle intelligence has been proposed in Ref. [26]. Our paper will use that process and enrich it, placing it in a larger context and therefore scaling it up as part of a whole in-vehicle management system integrating additional knowledge and intelligence layers with the use of neural networks. The algorithm results are used to investigate the safety and reliability issues existing in the proposed functionality. Therefore, we assume that the algorithmic process below has already knowledge of the associated risks with any decision (as an outcome of our work in Ref. [26]) and considers only low-risk decisions and so forth.

### 3.2.1. Least Safety Distance Warning

This function will provide an alert when the vehicle reaches a least safety distance  $d_{safe}$ , while maintaining a velocity above a specific threshold  $u_{threshold}$ .

If  $M$  is a genuine subset of  $N$  such that Equation (10):

$$M = \left\{ m \in N : u_0 > u_{threshold} \wedge d_m \in D \wedge d_m < d_{safe} \right\} \tag{10}$$

Therefore, the genuine subset of vehicles  $V_{WARN}$  that may reach the safety distance is given by Equation (11):

$$V_{WARN} = \{v_i \in V, \forall i \in M\} \tag{11}$$

The warning function is defined as Equation (12):

$$F = \begin{cases} \text{"WARNING"}, & V_{WARN} \neq \emptyset \\ \text{"NO WARNING"}, & V_{WARN} = \emptyset \end{cases} \tag{12}$$

Additional warning levels and corresponding messages can be easily created e.g., "DANGER", "WARNING", "CAUTION", "OK", by using multiple appropriate safety distances [27], as shown in the following table (Table 3).

**Table 3.** Warning level values (crisp set).

WarningLevelValues $w_i$	Safe Distance
"Danger"	0.8 $d_{safe}$
"Warning"	$d_{safe}$
"Caution"	1.5 $d_{safe}$
"OK"	2.0 $d_{safe}$

The Warning Function outputs can be also formulated into a fuzzy set, based on an array of membership functions, e.g., triangular, sigmoidal, z-shaped, bell-shaped, etc. The sigmoidal MF and the difference between the 2 sigmoidal MF are selected.

Sigmoidal MF is given by Equation (13):

$$sigmf(x, a, c) = \frac{1}{1 + e^{-a(x-c)}} \tag{13}$$

The parameters  $c$  and  $a$  represent the "center" (i.e., the position where the function has a value of 0.5) and the "slope" (i.e., how fast it drops from 1 to 0 around the "center") respectively. Sigmoidal Difference MF is given by Equation (14):

$$dsigmf(x, a, b, c_1, c_2) = \frac{1}{1 + e^{-a(x-c_1)}} - \frac{1}{1 + e^{-b(x-c_2)}} \tag{14}$$

The following membership functions are used to build the fuzzy set on Table 4 and its MF plot in Figure 4.

**Table 4.** Warning level values (fuzzy set).

WarningLevelValues $w_i$	Membership Function
“Danger”	$\text{sigmf}(x, 20, 1)$
“Warning”	$\text{dsigmf}(x, 30, 30, 1, 1.5)$
“Caution”	$\text{dsigmf}(x, 30, 30, 1.5, 2)$
“OK”	$\text{sigmf}(x, 20, 2)$



**Figure 4.** Membership function plot diagram.

### 3.2.2. Safe following Distance Warning

Our goal here would be to investigate whether a warning should be issued following the violation of a safety distance  $d_{front\_safe}$ .

We consider as  $u_0$  the speed of the reference vehicle at a given point in time and  $t_{reaction}$  the driver brake reaction time. The latter is considered as the time that elapses between the occurrence of the danger and the moment the vehicle stops. The brake reaction time depends on various parameters (e.g., age, gender, fatigue, etc.), with typical values ranging from 2.5 s to 1.4 s [28–30]. Next, we calculate the reaction distance, which is defined as the distance from recognizing the danger to where you begin to brake as follows Equation (15):

$$d_{reaction} = u_0 t_{reaction} \tag{15}$$

In case the forward vehicle  $v_i$  reduces its speed to  $u_i$ , apart from the reaction distance, account for the braking distance  $d_{braking}$  required by the subject vehicle to match its speed with the former should also be considered. Let  $m$  be the mass of the vehicle,  $g$  be the acceleration of gravity and  $\mu$  be the coefficient of kinetic friction between the tires and the road. The required reduction in kinetic energy is given by Equation (16):

$$\Delta E_{kinetic} = \frac{1}{2} m (u_i^2 - u_0^2) \tag{16}$$

where  $u_0$  is the initial speed and  $u_i$  the final speed of the vehicle.

This amount of energy must be absorbed by the braking system, which in turn is required to put a work of:

$$W_{braking} = -\mu mg d_{braking}$$

where  $\mu$  is the kinetic friction coefficient,  $g$  is the gravitational constant,  $m$  is the mass of the vehicle and  $d_{braking}$  is the braking distance.

Solving the above formula over the (baseline) braking distance gives us Equation (17):

$$d_{braking} = \begin{cases} \frac{u_0^2 - u_i^2}{2\mu g}, & u_0 > u_i \\ 0, & u_0 \leq u_i \end{cases} \tag{17}$$

To get an idea of the order of magnitude of the kinetic friction coefficient, we refer to the two tables below (Tables 5 and 6) which depict the different values of the kinetic friction coefficient for various surfaces [31–33].

**Table 5.** Average value of tire friction coefficient.

Road Surface	Peak Value	Sliding Value
Asphalt and concrete (dry)	0.80–0.90	0.75
Asphalt (wet)	0.50–0.70	0.45–0.60
Concrete (wet)	0.80	0.70
Gravel	0.60	0.55
Earth road (dry)	0.68	0.65
Earth road (wet)	0.55	0.40–0.50
Snow (hard-packed)	0.20	0.15
Ice	0.10	0.07

**Table 6.** Tire friction coefficient on asphalt.

Tire Friction Coefficient on Asphalt						
Vehicle Speed (km/h)	Tread Depth (mm)	Road Condition				
		Dry	Wet (Water Depth ≈ 0.2 mm)	Heavy Rainfall (Water Depth ≈ 1 mm)	Puddles (Water Depth ≈ 2 mm)	Ice (Black Ice)
50	New	0.85	0.65	0.55	0.50	≤0.10
50	1.6	1.00	0.50	0.40	0.25	≤0.10
90	New	0.80	0.60	0.30	0.05	
90	1.6	0.95	0.20	0.10	0.05	
130	New	0.75	0.55	0.20	0.00	
130	1.6	0.90	0.20	0.10	0.00	

To estimate the braking distance we take the assumption of the ideal braking force (friction) given by  $T = \mu mg$ . It should be noted that various factors may affect the coefficient  $\mu$ , such as temperature or humidity of the road, type of surface, condition of tires, etc. However, in our study for simplicity reasons we consider a constant value of the coefficient  $\mu$ .

Next, we calculate the least safe distance given by the addition of both the reaction and braking distances as shown below in Equation (18):

$$d_{front\_safe} = d_{reaction} + d_{braking} \tag{18}$$

Next, we consider a frontal “guard” of width  $L$ , as shown in Figure 5: which may have a constant value or a varying value, depending on the environmental/road conditions. The value of  $L$  can be obtained by the onboard road network GIS data or the V2I. For a given  $L$ , the maximum angular deviation  $\theta_{front\_max}$  from the reference vehicle’s current course in case of a frontal obstacle can be calculated, as depicted in Figure 4:

It can be derived from Figure 4 that Equation (19),

$$\theta_{front\_max} = \arctan\left(\frac{L}{2d_{front\_safe}}\right) \tag{19}$$

To this end, all vehicles that maintain a distance less than the safe distance together with an angular deviation up to  $\theta_{front\_max}$  from the reference vehicle’s course are considered possible forward collisions.

Similarly to Equation (1), we define the set MMM as Equation (20):

$$M = \left\{ m \in N : \begin{array}{l} d_m \in D \wedge d_m < d_{front\_safe} \\ \wedge \\ \theta_m \in \Theta \wedge |\theta_m| \leq \theta_{front\_max} \end{array} \right\} \tag{20}$$

It should be noted that there can be more warning level indications by using multiple appropriate values for  $d_{front\_safe}$ , as for example in Table 3 (crisp set) and Table 4 (fuzzy set).

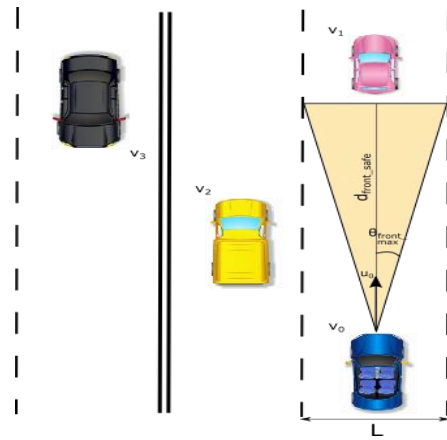


Figure 5. Calculation of maximum angular deviation.

### 3.2.3. Safe Front-Side Distance Warning

In this case, the objective resembles (b), however, the front-side areas of the vehicle are also considered. A safe distance  $d_{side\_safe}$  from each side of the vehicle (perpendicular to the vehicle’s direction) is defined as the half-width of the driving lane or some other appropriate value.

Considering Figure 6 we gather that the angular deviations  $\theta$  of the peer vehicles from the subject vehicle’s course are in the range Equations (21)–(23):

$$\theta \in (\theta_{front\_max}, \frac{\pi}{2}], \text{ for the right side} \tag{21}$$

and:

$$\theta \in [-\frac{\pi}{2}, -\theta_{front\_max}), \text{ for the left side} \tag{22}$$

or, all together:

$$\frac{\pi}{2} \geq |\theta| > \theta_{front\_max} \tag{23}$$

Similarly, the minimum front-side safe distance is defined by Equation (24):

$$d_{frontside\_safe} = \frac{d_{side\_safe}}{\cos(\frac{\pi}{2} - |\theta|)} \tag{24}$$

Let  $M$  be a genuine subset of  $N$  such that Equation (25):

$$M = \left\{ m \in N : \begin{array}{l} \theta_m \in \Theta \wedge \frac{\pi}{2} \geq |\theta_m| > \theta_{front\_max} \\ \wedge \\ d_m \in D \wedge d_m < \frac{d_{side\_safe}}{\cos(\frac{\pi}{2} - |\theta_m|)} \end{array} \right\} \tag{25}$$

The set of vehicles  $V_{WARN}$  that constitute safety hazards for impacts from the front side as well as the warning function  $F$  are defined as in Equations (1) and (2).

### 3.2.4. Congestion Ahead Warning

Next, we propose another warning function with the aim to generate alerts based on congestion in the front of the road. In this case, the term congestion can be defined as the number of vehicles above a given threshold per unit of road segment area, or simply as “high vehicle density”.



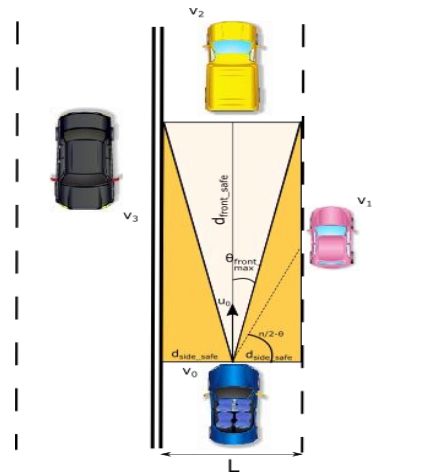


Figure 6. Maximum angular deviation based on monitoring the front-side areas of the vehicle.

We assume a road, on which the subject vehicle is traveling, of known width  $W$  and a series of sample points  $S_i, i = 0, 1, 2, \dots$  of the road axis, with known coordinates  $(x_{S_i}, y_{S_i})$ . Sample point  $S_0$  is the closest road axis sample point to the subject vehicle’s location and direction at a given moment. The set of vectors  $\vec{S}$  formed by every two consecutive sample points  $S_i$  is defined as Equation (26):

$$\vec{S} = \{ \overrightarrow{S_i S_{i+1}} \}, \{ i = 0, 1, 2, \dots \} \tag{26}$$

Let  $A$  and  $B$  be the set of points on the right and left side of the road respectively, defined as Equation (27):

$$A = \{ A_i \}, B = \{ B_i \} \text{ such that } \overline{A_i B_i} \perp \overline{S_i S_{i+1}} \tag{27}$$

Every point  $A_i$  and  $B_i$  have respective coordinates  $(x_{A_i}, y_{A_i})$  and  $(x_{B_i}, y_{B_i})$ . Figure 7 depicts the above concisely.

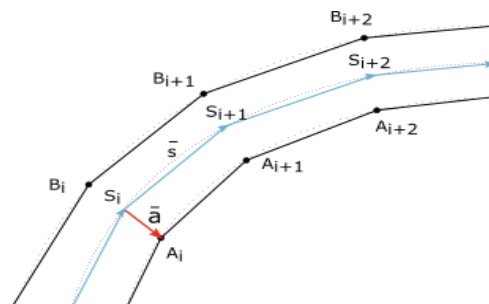


Figure 7. Calculation of congestion ahead warning (1st stage).

Our first goal is to find a formula to calculate the sets  $A$  and  $B$ .

Procedure:

Let Equations (28) and (29):

$$\vec{s} \equiv \overline{S_i S_{i+1}} = \begin{bmatrix} x_{S_{i+1}} - x_{S_i} \\ y_{S_{i+1}} - y_{S_i} \end{bmatrix} = \begin{bmatrix} s_x \\ s_y \end{bmatrix} \tag{28}$$

and:

$$\vec{a} \equiv \overline{S_i A_i} = \begin{bmatrix} x_{S_i} - x_{A_i} \\ y_{S_i} - y_{A_i} \end{bmatrix} = \begin{bmatrix} a_x \\ a_y \end{bmatrix} \tag{29}$$

If  $L_S$  (sampling length) is the road length between two consecutive points of the road network (it is available from the onboard GIS data), then  $L_S = \text{arc}(S_i S_{i+1})$ .

However, we can acquire a sufficiently small sampling length, by performing a linear or spline interpolation between the sampling points of the road segment, such that  $S_i S_{i+1} \approx \text{arc}(S_i S_{i+1})$ . Therefore we have Equation (30):

$$|\bar{s}| = \sqrt{s_x^2 + s_y^2} \approx L_S \tag{30}$$

The length of vector  $\bar{a}$  is approximately equal to half the road width, given the small sampling length Equation (31).

$$|\bar{a}| = \sqrt{a_x^2 + a_y^2} \approx \frac{W}{2} \tag{31}$$

The vectors  $\bar{s}$  and  $\bar{a}$  are vertical. Thus, the triangle  $A_i B_i S_{i+1}$  on Figure 4 is isosceles, with a base length  $|\bar{a}|$ , height  $|\bar{s}|$  and can be considered as the result of a rotation by a positive angle  $\theta$ , where  $\theta$  the angle  $\widehat{i, S_i S_{i+1}}$ , and a translation by  $(x_{S_i}, y_{S_i})$  of a triangle with its base midpoint set at  $(0, 0)$  and its vertex angle bisector on the positive  $x$ -axis.

The coordinates  $(x_{A_i}, y_{A_i})$  and  $(x_{B_i}, y_{B_i})$  are respectively Equation (32):

$$\begin{bmatrix} x_{A_i, B_i} \\ y_{A_i, B_i} \end{bmatrix} = \begin{bmatrix} x_{S_i} \\ y_{S_i} \end{bmatrix} + \begin{bmatrix} \cos \theta & -\sin \theta \\ \sin \theta & \cos \theta \end{bmatrix} \cdot \begin{bmatrix} 0 \\ \mp W/2 \end{bmatrix} \tag{32}$$

Substituting  $\sin \theta \approx \frac{s_y}{L_S}$  and  $\cos \theta = \frac{s_x}{L_S}$  we get Equations (33) and (34):

$$x_{A_i, B_i} = x_{S_i} \pm \frac{W}{2L_S} s_y \tag{33}$$

and:

$$y_{A_i, B_i} = y_{S_i} \mp \frac{W}{2L_S} s_x \tag{34}$$

In order to calculate the existence of traffic congestion at a road distance of  $L_{ahead}$  from the location of the subject vehicle, we will count the number of vehicles  $N_{window}$  inside a road segment “window” of length  $L_{window}$ , as shown in Figure 8.

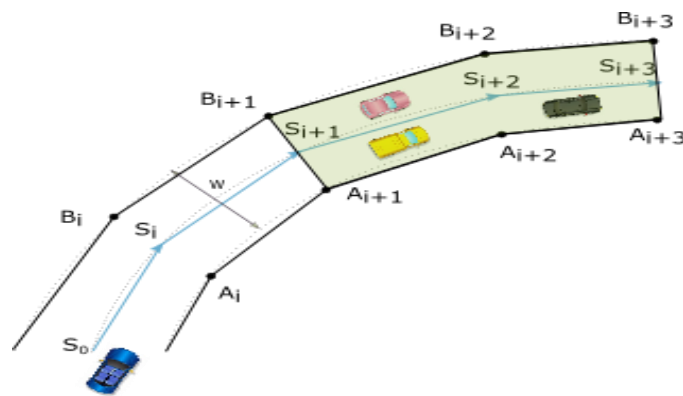


Figure 8. Calculation of congestion ahead warning (2nd stage).

Let points  $S_j, S_k \in S$  be the sample points closest to the start and end of the window respectively.

We can derive  $j$  and  $k$  by Equations (35) and (36):

$$j \in \{1, 2, 3, \dots\} : \sum_{i=0}^{j-1} |\overline{S_i S_{i+1}}| \approx L_{ahead} \tag{35}$$

and:

$$k \in \{2, 3, \dots\} : j < k \wedge \sum_{i=j}^{k-1} |S_i S_{i+1}| \approx L_{window} \tag{36}$$

The window (road segment) can be approximated by the simple polygon defined by the vertices Equation (37):

$$Window\ polygon = A_j \dots A_k B_k \dots B_j \tag{37}$$

To make the polygon notation easier, we can define a new set of vertices C, such that Equation (38):

$$C_0 \equiv A_j, \dots, C_{k-j} \equiv A_k, C_{k-j+1} \equiv B_k, \dots, C_{2(k-j)+1} \equiv B_j \tag{38}$$

So Equation (39):

$$Window\ polygon = C_0 \dots C_{2(k-j)+1} \tag{39}$$

The Jordan Curve Theorem can give us the number of peer vehicles per window, while the area  $S_{window}$  of the window polygon can be found by the following Equation (40):

$$S_{window} = \frac{1}{2} \sum_{i=0}^{2(k-j)} (x_{C_{i+1}} + x_{C_i})(y_{C_{i+1}} - y_{C_i}) \tag{40}$$

The space that is occupied by every vehicle inside the window is given by the following formula,  $L_{v_i}$  is its exchanged length with the subject vehicle Equation (41):

$$S_{vehicles} = \sum_{i=1}^{N_{window}} (1 + c_{spacing}) L_{v_i} \cdot L \tag{41}$$

where the positive coefficient  $c_{spacing}$  translates to how many car-lengths is the minimum distance (“bumper-to-bumper”) between the congested vehicles in the window.

The congestion on the window of length  $L_{Window}$ , at a road distance of  $L_{ahead}$  ahead on the traveling direction of the subject vehicle, is Equation (42):

$$Congestion\ [\%] = \frac{S_{vehicles}}{S_{window}} \times 100\% \tag{42}$$

#### 4. Simulation Results

##### 4.1. Simulator Setup

In order to prove that our algorithms are sound and practically applicable for industrial purposes, we would ideally have a controlled traffic environment where the motion parameters (location, speed, etc.) of each participating vehicle are known, and the results are evaluated and verified multiple times.

All simulations are developed in C# programming language, under the .NET Framework 4.6, and the Microsoft Windows OS and x86/x64 while the WPF framework was used for the graphical interface. The RuyJIT compiler from Microsoft Corp. was used, which takes advantage of the hardware and specific central processing unit (CPU) instructions that improve performance. Multithreading is implemented by our simulator for greater efficiency in the calculations required.

This section presents results springing from the simulator’s operation, whereas a snapshot of its Graphical User Interface (GUI) is given in Figure 9.

For a consistent road segment of a given length, width, and lane number, we place a specific number of vehicles along the length of every lane, following the normal distribution. We also ensure that the vehicles do not overlap due to their dimensions. Additionally, we set a minimum deviation of the vehicle’s center from the lane’s axis, which also follows a Gaussian distribution, in order to achieve more realistic results.



Figure 9. Software simulator GUI.

In our study, we consider four different types of vehicles of different sizes and occurring probability. Those are (a) passenger cars, (b) light trucks, (c) trucks or buses, (d) heavy trucks). The first three warning functions are tested for every type of the above-mentioned vehicles, grouping them by intervals (bins), e.g., every 5% of the total road length. The results of the average warning function distribution are presented in a histogram. Then, the process is then repeated 100 K times until the average values for every bin are extracted.

4.2. Results

For our simulations, we assume a road segment of 1000 m in length, and 20 m in width, with 4 lanes of 5 m each and a lane-axis standard deviation of 0.75 m. The occurrence probabilities for every type of vehicle are selected as follows: 80% for passenger vehicles (3–5 m length), 10% for light trucks (5–7 m length), 7% for buses (7–11 m length) and 3% for heavy trucks (11 to 16 m length).

Warning Function 1—Proximity Warning

This section examines the effect of traffic density on the proximity warning and particularly the distribution along the road. We use a (theoretical) Gaussian distribution of traffic  $N(\mu, \sigma)$  with a center at 500 m and a standard deviation  $\sigma = 150$  m ( $N(500, 150)$ ), with a variable number of vehicles per lane.

Figure 10 depicts the results of our study. As expected, high congregations of vehicles at the center of the distribution (500 m) cause similar increases in the percentage of vehicles experiencing proximity warnings.

Warning Function 2—Safe following Distance Warning

Next, the results of the implementation of the safe following distance warning function are presented. In Figure 11, we study the effect of the desired speed (max. speed) on the warning function results. The vehicle distribution and speed profiles are derived from an LWR model simulation of an initial standstill in the 200–300 m range (e.g., traffic light) and the calculation of the traffic, moments after it is restored.

In the beginning, we observe a low warning level of 500–1000 m for the first cars to go. This is reasonable since those cars have no other vehicle ahead. Next, as vehicles are increasing their speed at 300–500 m, we observe increased warning levels.

It should be noted here, that the according to the LWR model, the local speed will instantaneously follow the traffic density, therefore it is expected that the warning levels in this scenario will be slightly different than in real traffic conditions.

Next, we will examine the effect that a Gaussian traffic distribution imposes on the safe following warning (Figure 12). It can be concluded that an increasing number of vehicles leads to a growth in the safe following warning levels with a similar distribution.

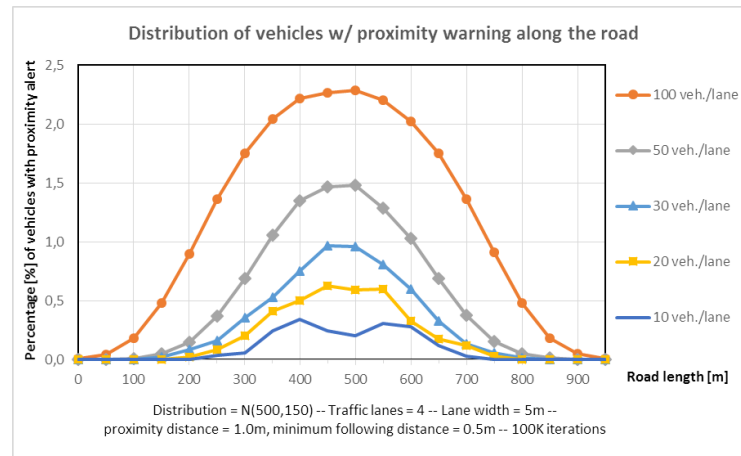


Figure 10. Effect of traffic density to proximity warning values.

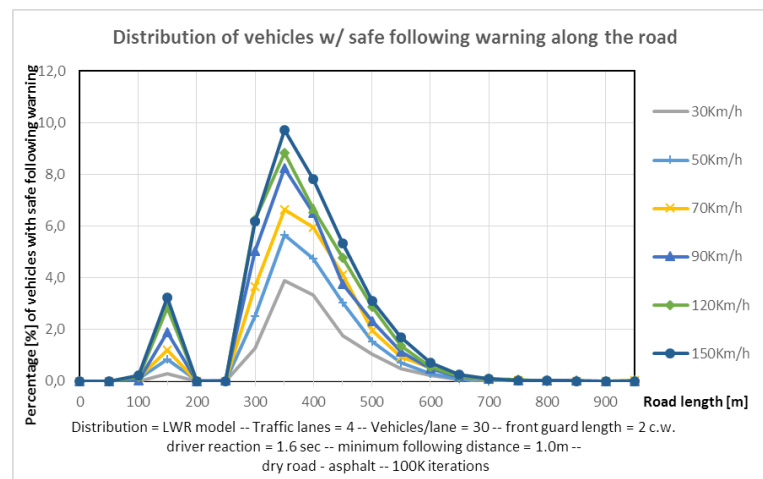


Figure 11. Effect of desired speed to safe following warning values using LWR model distribution.

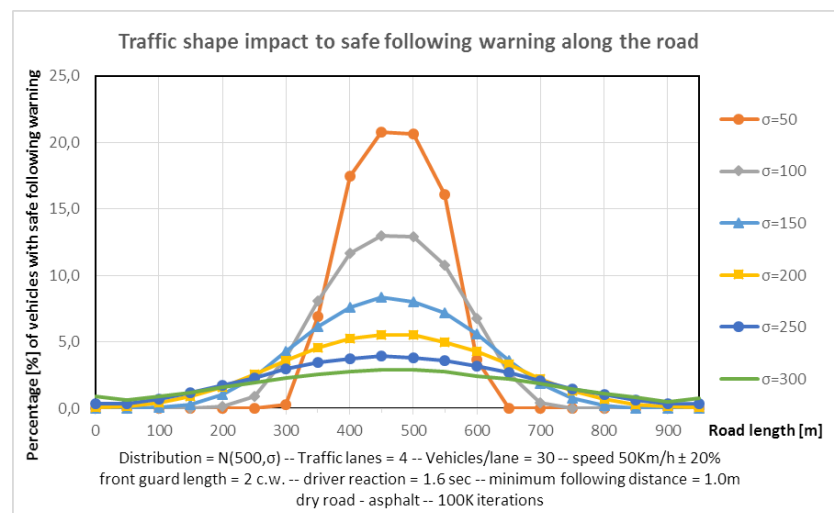


Figure 12. Effect of traffic shape to safe following warning values.

Following we will consider the impact of the driver’s reaction time on following safety precautions using the LWR simulation as above, as shown in Figure 13.

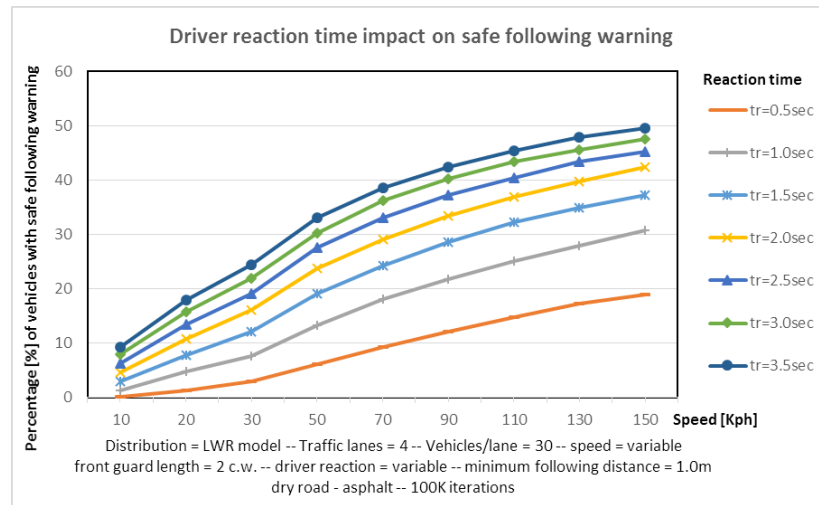


Figure 13. Impact of driver reaction time to safe following warning values at various speeds using LWR model distribution.

From our simulations, it is evident that a driver with a considerably high reaction time above 2.5 s, such as an intoxicated driver would cause a considerable raise in the safe following warning value. It should be also noted that assuming a very alert driver with a reaction time of 1.0 s, we can study the effect of the minimum following distance (“bumper-to-bumper”) in the safe following values, as shown in Figure 14.



Figure 14. Effect of minimum following distance to safe following warning values at various speeds using LWR traffic distribution.

Based on these results, it can be assumed that regardless of the rate of reaction of the driver, at very high velocities (>150 Kph) the safe following warnings will be raised, despite the distance that is kept from the following car.

Warning Function 3—Safe Front-Side Distance Warning



In this section, the outcomes of the front-side distance warning function are examined. Maintaining the same assumptions as in the previous paragraph, we also consider the front-side distance given by Equation (43).

$$d_{front\_side\_safe} = \frac{1}{2}d_{front\_safe} \tag{43}$$

Next, in Figure 15 for different values of speed, we study the effect of the vehicle deviation from the axis of the lane, on which it is moving, to the safe front-side distance warning values. From our observations, it is evident that when all vehicles travel right on the axes of their lanes ( $\sigma = 0$ ), there are no lateral warnings.

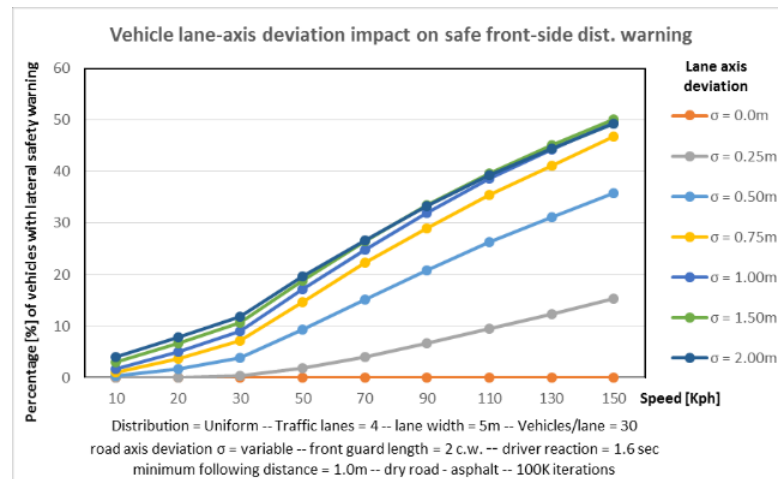


**Figure 15.** Effect of vehicle lane-axis deviation on safe front-side distance warning at various speeds in uniform traffic distribution.

However, as the deviations increase, so do the safe side distance warnings, but only up to a point ( $\sigma = 0.75$  m). After that point, they reach a limit since the deviations are so big that vehicles have moved to the adjacent lane, becoming frontal obstacles to nearby vehicles. Another remark arises if we examine a special case from the previous result when, for example,  $\sigma = 0.50$  m and the lane length varies. This is depicted in Figure 16, where it can be observed that the percentage of vehicles with safe front-side distance warning increases as the lane width decreases. The effect is more severe at higher speeds.

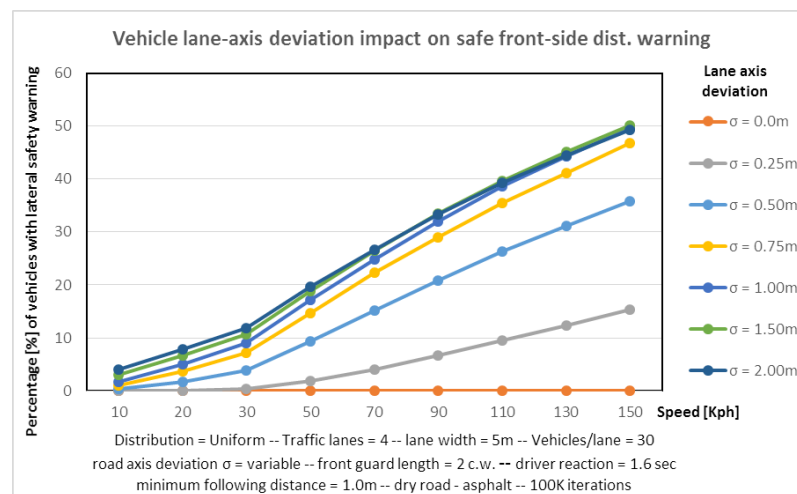


**Figure 16.** Effect of lane width in safe front-side distance warning at various speeds in a uniform traffic distribution, when  $\sigma^2 = 0.5$  m.

### Warning Function 4—Congestion ahead warning

In this paragraph, we will assess the effectiveness of our congestion ahead warning function by means of a statistical test evaluation. Since it would be difficult to present results for the congestion ahead for each vehicle in the traffic, we decided to place a subject vehicle at the beginning of the road segment (0 m) and run the congestion ahead algorithm using a sliding congestion window of length, e.g.,  $L_{window} = 30$  m along the road segment. The sampling length of the road axis was arbitrarily chosen at  $L_s = 10$  m. So the first window is evaluated at 0–30 m, the second at 10–40 m, and so forth, producing a set of numbers denoting the “congestion profile”.

For this purpose, we perform a  $X^2$  test with 1 degree of freedom, in order to check the independence (null hypothesis) of the two. We use the value of  $X^2$  to display the probability  $p$  of rejecting the null hypothesis. To put it best, if the distribution of the congestion profile data is left entirely to chance, we have probability  $p$  of finding a dependency between the congestion profile and the actual vehicle distribution. By convention, values of  $p > 0.95$  are considered to be a quite reasonable probability that we have a dependency between the observed and the expected distributions. We study a Gaussian traffic distribution  $N(500, 150)$  with 20 vehicles/lane, with a minimum following distance of 0.5 m. In Figure 17, we use two traffic lanes and a small congestion window of 10 m. This is the reason for the “erratic” behavior of the congestion profile line. It is following the underlying vehicle distribution fairly closely ( $p = 0.976$ ).

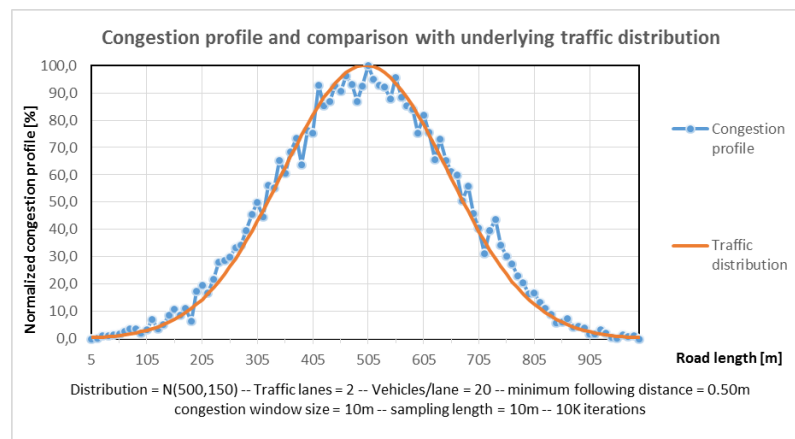


Figure 17. Congestion profile comparison with underlying traffic distribution,  $p = 0.976$ .

In Figure 18, we increase the congestion window length to 30 m. The congestion profile is more “smooth”, as expected. The dependency is still quite high ( $p = 0.989$ ).

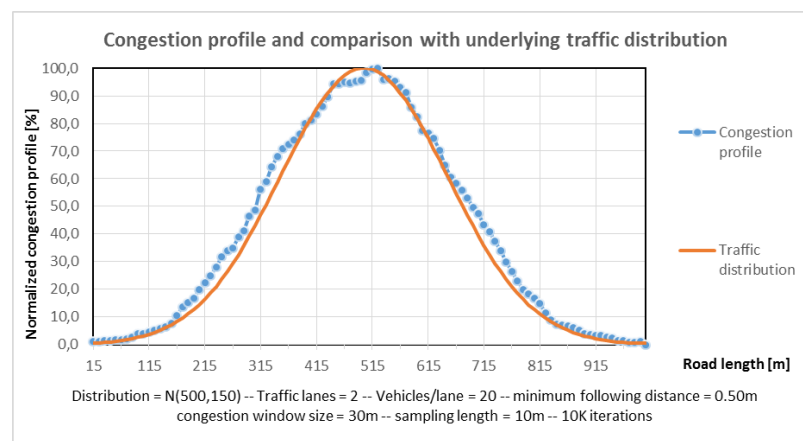


Figure 18. Congestion profile comparison with underlying traffic distribution,  $p = 0.989$ .

In Figure 19, we use four lanes of traffic. Last, in Figure 20 we run a test using a uniform distribution with 4 traffic lanes and 30 m congestion size ( $p = 0.999$ ).

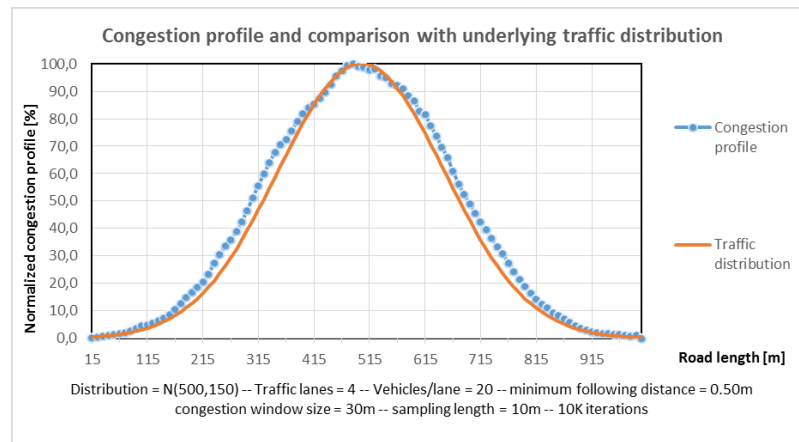


Figure 19. Congestion profile comparison with underlying traffic distribution,  $p = 0.979$ .

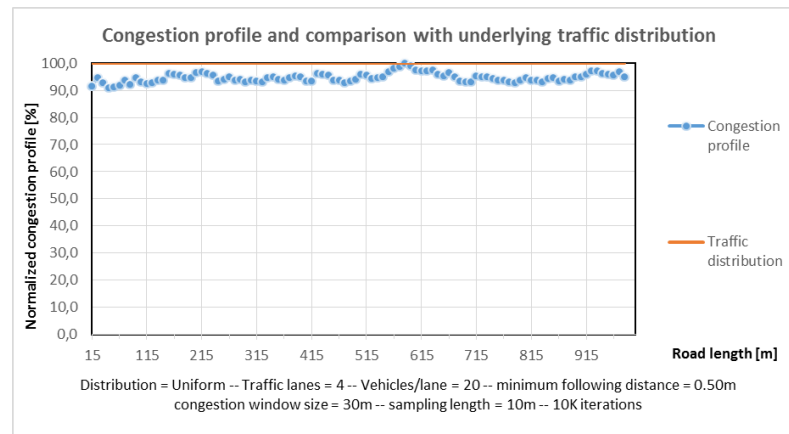


Figure 20. Congestion profile comparison with underlying traffic distribution,  $p = 0.999$ .

### 5. Conclusions and Future Directions

Numerous theories have been proposed as facilitators of V2X communications, offering breakthrough management capabilities for traffic conditions, or emergency situations. However, most of them lack dependability and cost-effectiveness, as they depend upon unreliable technologies and high infrastructure overhead.

This work presented a framework that operates on the idea of collecting information from various sources through vehicular sensor networks, in turn exploiting the sensors already embedded in vehicles. This data is intelligently processed, integrating knowledge and past experience, even associating candidate decisions with risks and considering only the low-risk ones, in order to issue directives to the driver, and hence proactively safeguarding the vehicle and alerting the driver for upcoming emergency events. Our method has been assessed by the implementation of a novel heuristic function that proves efficient for reaching decisions that protect the driver and the vehicle in emergency situations. Extensive simulation results exhibit the efficiency and scalability of our method.

Several exciting areas are yet to be addressed. Firstly, ASM can be upgraded to include more accurate sensors (e.g., proximity sensors, speedometer, accelerometer, etc.). In doing so, we can increase our measurement accuracy and also transmit the information of misbehaving drivers in the group, as well as study non-obvious, cognitive drivers' reactions (e.g., sudden brake) which could affect the algorithm's effectiveness. Second, ASM can be combined with studies on the percentage of instrumented vehicles that affects the algorithm's efficiency. Third, ASM can integrate information originating from sources

such as mobile communication networks (4G, 5G-D2D, etc.) increasing its availability and reliability further.

**Author Contributions:** Conceptualization, T.Z.; Investigation, K.K.; Methodology, E.P. (Elena Politi); Project administration, E.P. (Elias Panagiotopoulos); Supervision, G.D. All authors have read and agreed to the published version of the manuscript.

**Funding:** This research received no external funding.

**Institutional Review Board Statement:** Not applicable.

**Informed Consent Statement:** Not applicable.

**Data Availability Statement:** Not applicable.

**Conflicts of Interest:** The authors declare no conflict of interest.

## References

1. Rocha Filho, G.P.; Meneguette, R.I.; Neto, J.R.T.; Valejo, A.; Weigang, L.; Ueyama, J.; Pessin, G.; Villas, L.A. Enhancing intelligence in traffic management systems to aid in vehicle traffic congestion problems in smart cities. *Ad. Hoc. Netw.* **2020**, *107*, 102265. [CrossRef]
2. United Nations. Transforming Our World: The 2030 Agenda for Sustainable Development. Available online: <https://sustainabledevelopment.un.org/content/documents/21252030%20Agenda%20for%20Sustainable%20Development%20web.pdf> (accessed on 10 July 2022).
3. United Nations. The 17 Goals. Available online: <https://sdgs.un.org/goals> (accessed on 15 July 2022).
4. European Commission. EU Road Safety Policy Framework 2021–2030-Next Steps towards Vision Zero. Available online: <https://ec.europa.eu/transport/sites/transport/files/legislation/swd20190283-roadsafety-vision-zero.pdf> (accessed on 15 July 2022).
5. Zographos, T.; Dimitrakopoulos, G.; Anagnostopoulos, D. Driver Assistance through an Autonomous Safety Management Framework. In Proceedings of the IEEE Wireless and Mobile Communications (WiMOB) 2016, New York, NY, USA, 17–19 October 2016.
6. Lu, N.; Cheng, N.; Zhang, N.; Shen, X.; Mark, J.W. Connected Vehicles: Solutions and Challenges. *IEEE Internet Things J.* **2014**, *1*, 289–299. [CrossRef]
7. Sedjelmaci, H.; Senouci, S.M.; Abu-Rgheff, M.A. An Efficient and Lightweight Intrusion Detection Mechanism for Service-Oriented Vehicular Networks. *IEEE Internet Things J.* **2014**, *1*, 570–577. [CrossRef]
8. Zhu, Y.H.; Luan, S.; Leung, V.C.; Chi, K. Enhancing Timer-Based Power Management to Support Delay-Intolerant Uplink Traffic in Infrastructure IEEE 802.11 WLANs. *IEEE Trans. Veh. Technol.* **2015**, *64*, 386–399. [CrossRef]
9. Schakel, W.J.; van Arem, B. Improving Traffic Flow Efficiency by In-Car Advice on Lane, Speed, and Headway. *IEEE Trans. ITS* **2014**, *15*, 1597–1606. [CrossRef]
10. Na, X.; Cole, D.J. Game-Theoretic Modeling of the Steering Interaction Between a Human Driver and a Vehicle Collision Avoidance Controller. *IEEE Trans. Hum.-Mach. Syst.* **2015**, *45*, 25–38. [CrossRef]
11. Lin, J.R.; Talty, T.; Tonguz, O.K. A Blind Zone Alert System Based on Intra-Vehicular Wireless Sensor Networks. *IEEE Trans. Ind. Inform.* **2015**, *11*, 476–484. [CrossRef]
12. Sun, Y.; Chowdhury, K. Enabling emergency communication through a cognitive radio vehicular network. *IEEE Commun. Mag.* **2014**, *52*, 68–75. [CrossRef]
13. Lee, W.H.; Lai, Y.C.; Chen, P.Y. A Study on Energy Saving and CO<sub>2</sub> Emission Reduction on Signal Countdown Extension by Vehicular Ad Hoc Networks. *IEEE Trans. Veh. Technol.* **2015**, *64*, 890–900. [CrossRef]
14. Dimitrakopoulos, G.; Bravos, G.; Nikolaidou, M.; Anagnostopoulos, D. A Proactive, Knowledge-Based Intelligent Transportation System based on Vehicular Sensor Networks. *IET Intell. Transp. Syst. J.* **2013**, *7*, 454–463. [CrossRef]
15. Lin, J.R.; Talty, T.; Tonguz, O.K. On the potential of bluetooth low energy technology for vehicular applications. *IEEE Com. Mag.* **2015**, *53*, 267–275. [CrossRef]
16. Dimitrakopoulos, G.; Ghattas, J. Autonomic Decision Making for Vehicles based on Visible Light Communications. In Proceedings of the 14th Wireless Telecommunications Symposium (WTS) 2015, New York, NY, USA, 15–17 April 2015.
17. Ferreira, M.; d’Orey, P.M. On the Impact of Virtual Traffic Lights on Carbon Emissions Mitigation. *IEEE Trans. ITS* **2012**, *13*, 284–295. [CrossRef]
18. Sinha, R.; Roop, P.; Ranjitkar, P. Virtual Traffic Lights+: A Robust, Practical, and Functionally Safe Intelligent Transportation System. *Transp. Res. Rec.* **2013**, 2381. [CrossRef]
19. Bellotti, F.; Berta, R.; Kobeissi, A.; Osman, N.; Arnold, E.; Dianati, M.; Nagy, B.; De Gloria, A. Designing an IoT Framework for Automated Driving Impact Analysis. In Proceedings of the 2019 IEEE Intelligent Vehicles Symposium (IV), Paris, France, 9–12 June 2019; pp. 1111–1117. [CrossRef]
20. An, D.; Liu, J.; Zhang, M.; Chen, X.; Chen, M.; Sun, H. Uncertainty Modeling and Runtime Verification for Autonomous Vehicles Driving Control: A Machine Learning-based Approach. *J. Syst. Softw.* **2020**, *167*, 110617. [CrossRef]

21. Panagiotopoulos, I.; Karathanasopoulou, K.; Dimitrakopoulos, G. Risk Assessment in the Context of Dynamic Reconfiguration of Driving Automation Level in Highly Automated Vehicles. In Proceedings of the 7th IEEE Conference on Computational Science & Computational Intelligence (CSCI), Las Vegas, NV, USA, 15–17 December 2021.
22. Yan, L.; Wu, C.; Zhu, D.; Ran, B.; He, Y.; Qin, L.; Li, H. Driving Mode Decision Making for Intelligent Vehicles in Stressful Traffic Events. *Transp. Res. Rec. J. Transp. Res. Board* **2017**, *2625*, 9–19. [[CrossRef](#)]
23. Panagiotopoulos, K.I.; Karathanasopoulou, G.; Dimitrakopoulos, G. Risk based Decision Making Functionality for Improving the Level of Autonomy Reconfiguration in Automated Vehicles. In Proceedings of the ITS World Congress 2022, Los Angeles, NV, USA, 18–22 September 2022.
24. Li, X.; Zhang, X.; Ren, X.; Fritsche, M.; Wickert, J.; Schuh, H. Precise positioning with current multi-constellation Global Navigation Satellite Systems: GPS, GLONASS, Galileo and BeiDou. *Sci. Rep.* **2015**, *5*, 8238. [[CrossRef](#)] [[PubMed](#)]
25. Jenny, B. Adaptive Composite Map Projections. *IEEE Trans. Vis. Comp. Graph.* **2012**, *18*, 2575–2582. [[CrossRef](#)] [[PubMed](#)]
26. Press, W.H.; Teukolsky, S.A.; Vetterling, W.T.; Flannery, B.P. *Numerical Recipes*, 3rd ed.; Cambridge Press: Cambridge, UK, 2007; pp. 1122–1124.
27. Green, M. “How long does it take to stop?” Methodological Analysis of Driver Perception-Brake Times. *Transp. Human Factors* **2000**, *2*, 195–216. [[CrossRef](#)]
28. Xing, C.F.; Yang, L.; Zhang, Y.H. Study of driver’s reaction time (DRT) during car following. In *Applied Mechanics and Materials*; Trans Tech Publications Ltd.: Wollerau, Switzerland, 2015; Volume 713–715.
29. D’Addario, P.M. *Perception-Response Time to Emergency Roadway Hazards and the Effect of Cognitive Distraction*; University of Toronto: Toronto, ON, Canada, 2014.
30. Wong, J.Y. *Theory of Ground Vehicles*, 4th ed.; Wiley: Hoboken, NJ, USA, 2008.
31. Robert Bosch GmbH. *Automotive Handbook*, 9th ed.; Robert Bosch GmbH: Gerlingen, Germany, 2014.
32. Treiber, M.; Kesting, A. *Traffic Flow Dynamics: Data, Models and Simulation*; Springer: Berlin/Heidelberg, Germany, 2013.
33. Edwards, D.J.; Holt, G.D.; Spittle, P.G. Guidance on Brake Testing for Rubber-Tyred Vehicles Operating in Quarries, Open Cast Coal Sites and Mines. 2007. Available online: <https://www.osti.gov/etdeweb/biblio/21396714> (accessed on 15 July 2022).